Covalent Linking of Near-Infrared Luminescent Ternary Lanthanide (Er^{3+}, Nd^{3+}, Yb^{3+}) Complexes on Functionalized Mesoporous MCM-41 and SBA-15

Li-Ning Sun,[†,‡] Hong-Jie Zhang,*[,†] Chun-Yun Peng,[†,‡] Jiang-Bo Yu,[†] Qing-Guo Meng,[†] Lian-She Fu,[†] Feng-Yi Liu,[†] and Xian-Min Guo[†,‡]

Key Laboratory of Rare Earth Chemistry and Physics, Changchun Institute of Applied Chemistry, Chinese Academy of Sciences, Changchun 130022, P. R. China, and Graduate School of the Chinese Academy of Sciences, Beijing, P. R. China.

Received: January 19, 2006; In Final Form: February 21, 2006

The near-infrared (NIR) luminescent lanthanide ions, such as Er(III), Nd(III), and Yb(III), have been paid much attention for the potential use in the optical communications or laser systems. For the first time, the NIR-luminescent $Ln(dbm)_3phen$ complexes have been covalently bonded to the ordered mesoporous materials MCM-41 and SBA-15 via a functionalized phen group phen−Si (phen−Si = 5-(*N*,*N*-bis-3-(triethoxysilyl)-propyl)ureyl-1,10-phenanthroline; dbm = dibenzoylmethanate; Ln = Er, Nd, Yb). The synthesis parameters $X = 12$ and $Y = 6$ h (X denotes $Ln(dbm)_3(H_2O)_2$/phen−MCM-41 molar ratio or $Ln(dbm)_3(H_2O)_2$/phen−SBA-15 molar ratio and Y is the reaction time for the ligand exchange reaction; phen−MCM-41 and phen−SBA-15 are phen-functionalized MCM-41 and SBA-15 mesoporous materials, respectively) were selected through a systematic and comparative study. The derivative materials, denoted as $Ln(dbm)_3$phen−MCM-41 and $Ln(dbm)_3$phen−SBA-15 (Ln = Er, Nd, Yb), were characterized by powder X-ray diffraction, nitrogen adsorption/desorption, Fourier transform infrared (FT-IR), elemental analysis, and fluorescence spectra. Upon excitation of the ligands absorption bands, all these materials show the characteristic NIR luminescence of the corresponding lanthanide ions through the intramolecular energy transfer from the ligands to the lanthanide ions. The excellent NIR-luminescent properties enable these mesoporous materials to have potential uses in optical amplifiers (operating at 1.3 or 1.5 μm), laser systems, or medical diagnostics. In addition, the $Ln(dbm)_3$phen−SBA-15 materials show an overall increase in relative luminescent intensity and lifetime compared to the $Ln(dbm)_3$phen−MCM-41 materials, which was explained by the comparison of the lanthanide ion content and the pore structures of the two kinds of mesoporous materials in detail.

1. Introduction

Near-infrared (NIR) emitting lanthanide ions, such as erbium (Er^{3+}), neodymium (Nd^{3+}), and ytterbium (Yb^{3+}), exhibit characteristic emission wavelengths with large Stokes shifts. These properties, coupled with the advantages of signal transmittance of NIR radiation, make them attractive for potential use in a number of applications. Recent interest in the photophysical properties of these lanthanide ions stems from their possible use in medical diagnostics because the longer emission wavelengths penetrate human tissue far more effectively than does UV or visible light.[1] In addition, NIR luminescence from lanthanide ions such as Nd(III) and Er(III) is used as the basis for the optical amplifiers used in fiber-optic systems based on silica fibers that transmit their signals in the 1300−1550 nm region.[2] However, it is difficult to generate this luminescence by direct excitation of these NIR-luminescence lanthanide ions due to their poor absorption abilities. To enhance absorption, lanthanide ions are chelated with organic ligands that have broad, intense absorption bands in the UV region. The ion-centered luminescence originates from the intramolecular energy transfer through the excited state of the ligand to the emitting level of the lanthanide ion. This is the so-called "antenna effect".[3]

For practical applications in optical devices, it is advantageous to incorporate these lanthanide complexes in an inert host matrix, for example, silica-based materials,[4] polymers,[5] or liquid crystal.[6] In the past few years, micelle-templated silicas have started to attract much attention as mesostructured hosts for optical functionalities. Since the mesoporous silica materials were first introduced in 1992,[7] the development of ordered mesoporous molecular sieves has been of widespread interest in materials science. Ordered mesoporous materials with unique properties (high surface area, ordered pore structure of varying morphologies, and controllable pore size over wide ranges) continue to be widely investigated because of their many potential applications in catalysis, adsorption and sensing, etc.[8] Recently, one of particular interest is the use of the ordered mesoporous silica material as a support for lanthanide complexes. Mesostructured materials offer the rigidity and photostability and, at the same time, have a well-defined hydrophilic/hydrophobic phase separation allowing for more sophisticated tuning of the lanthanide complex microenvironment. However, many studies were mainly focused on doping the mesoporous silica materials with the lanthanide complexes in which only weak physical interactions (van der Waals force, hydrogen bonding, or weak static effect) exist between the lanthanide complexes and the mesoporous materials.[9] This will give little control over the clustering

* To whom correspondence should be addressed. E-mail: hongjie@ns.ciac.jl.cn. Telephone: +86-431-5262127. Fax: +86-431-5698041.

[†] Changchun Institute of Applied Chemistry, Chinese Academy of Sciences.

[‡] Graduate School of the Chinese Academy of Sciences.

10.1021/jp060395u CCC: $33.50
Published on Web 03/23/2006

of emitting centers and lead to inhomogeneous dispersion of the components and leaching of the photoactive molecules in the obtained materials. Recently, our group has reported the syntheses of luminescent mesoporous material MCM-41 covalently bonded with a binary europium complex with phen ligand (Eu−phen−MCM-41, phen = 1,10-phenanthroline),[10] and the luminescent mesoporous material SBA-15 covalently bonded with a ternary lanthanide complex $Eu(tta)_3phen$ (tta = 2-thenoyltrifluoroacetonate) via a co-condensation method and a ligand exchange reaction.[11] These approaches enable a higher and more homogeneous surface coverage of organosilane functionalities and can effectively prevent the aggregation of lanthanide complexes. Moreover, compared with mesoporous material covalently bonded with the binary europium complex, the mesoporous material bonded with the $Eu(tta)_3phen$ complex shows improved luminescence behavior upon the introduction of β-diketonate ligand tta. And the ternary complex $Eu(tta)_3phen$ was evidenced to be covalently linked to the network of the mesoporous material successfully.

However, the lanthanide complexes that are covalently linked to a host matrix are mainly limited to the europium(III) and terbium(III) complexes.[10−12] The NIR-luminescent lanthanide complexes coupled to the host matrix via a covalently bonded group have been less well studied. Binnemans et al. reported the syntheses of covalently linking NIR-luminescence lanthanide complexes to a polymeric matrix through the phen-functionalized Merrifield resin[5a] and to a sol−gel matrix via the 2-substituted imidazo[4,5-*f*]-1,10-phenanthroline group,[13] and studied the NIR-luminescence properties of these materials. However, to the best of our knowledge, the syntheses and luminescence properties of mesoporous materials covalently bonded with NIR-luminescent lanthanide complexes have not been reported in the open literature so far.

Here, we extend our previous approach and present the systematic and comparative study of the mesoporous materials covalently bonded with erbium complexes designated as $Er(dbm)_3phen-MCM\text{-}41_{(X,Y)}$ (dbm = dibenzoylmethanate, phen−MCM-41 denotes phen-functionalized MCM-41 mesoporous material, X ranging from 1 to 14, and Y = 3, 6, 12, 18, and 24 h, respectively), where X denotes the $Er(dbm)_3(H_2O)$/phen−MCM-41 molar ratio and Y is the reaction time for the ligand exchange reaction. The analysis result shows that an optimum molar ratio (X = 12) and optimum reaction time (Y = 6) can be employed to synthesize the $Er(dbm)_3phen$−MCM-41 with a high loading of Er content yet a good mesostructure. So the reaction parameters (X = 12, Y = 6) were selected as the candidate for the syntheses of a series of mesoporous materials covalently bonded with NIR-luminescence lanthanide complexes, denoted as $Ln(dbm)_3phen$−MCM-41 and $Ln(dbm)_3phen$−SBA-15 (phen−SBA-15 denotes phen-functionalized SBA-15 mesoporous material, Ln = Er, Nd, Yb). Full characterization and detailed studies of NIR-luminescence properties of these mesoporous materials were investigated and compared.

2. Experimental Section

2.1. Materials. Tetraethoxysilane (TEOS, Aldrich), 3-(triethoxysilyl)-propyl isocyanate (Aldrich), triblock copolymer poly(ethylene glyco)-*block*-poly(propylene glycol)-*block*-poly(ethylene glycol) (Pluronic P123, $EO_{20}PO_{70}EO_{20}$, Aldrich), cetyltrimethylammonium bromide (CTAB, Aldrich), fuming nitric acid, and ethanol were used as received. The solvent chloroform ($CHCl_3$) was used after desiccation with anhydrous calcium chloride. Ytterbium oxide (Yb_2O_3, 99.99%), neodymium oxide (Nd_2O_3, 99.99%), and erbium oxide (Er_2O_3, 99.99%) were purchased from Yue Long Chemical Plant (Shanghai, China). 1,10-Phenanthroline monohydrate (phen·H_2O, 99%, AR), and dibenzoylmethane (Hdbm, CP) were bought from Beijing Fine Chemical Co. (Beijing, China).

$LnCl_3$ (Ln = Er, Yb, Nd) ethanol solution (EtOH) was prepared as follows: the rare earth oxide (Ln_2O_3) was dissolved in concentrated hydrochloric acid (HCl), and the surplus HCl was removed by evaporation. The residue was dissolved with anhydrous ethanol. The concentration of the rare earth ion was measured by titration with a standard ethylenediaminetetraacetic acid (EDTA) aqueous solution.

2.2. Synthesis of Phen-Functionalized MCM-41 Mesoporous Material (phen−MCM-41). The phen−MCM-41 was synthesized mainly as described in our previous publication with some minor modification.[10] The starting reagent 5-amino-1,10-phenanthroline (denoted as phen−NH_2) was prepared according to the procedure described in the literature.[14] The modified phenanthroline 5-(*N*,*N*-bis-3-(triethoxysilyl)propyl)-ureyl-1,10-phenanthroline (phen−Si) was synthesized by the reaction of phen−NH_2 and 3-(triethoxysilyl)-propyl isocyanate in $CHCl_3$ as described in ref 12b. Then CTAB (1.65 g) was dissolved in concentrated NH_3·H_2O (18 mL), to which deionized water (39 mL), TEOS (7.5 mL), and phen−Si (0.898 g) were added. The molar composition of the original synthetic mixture was phen−Si/TEOS/CTAB/NH_3·H_2O/H_2O = 0.04:1.0:0.139:3.76:66.57. The mixture was stirred for 7 h at room temperature and transferred into a Teflon bottle sealed in an autoclave, which was then heated at 90 °C for 24 h. Then the solid product was filtered, washed with H_2O, and dried for 12 h at 60 °C. The surfactant was removed by acid/solvent extraction, using a solution of 400 mL of ethanol and 7.3 mL of aqueous HCl (37%) per 5 g of sample. This mixture was refluxed for 7 h, then filtered and washed with EtOH until the pH was neutral. The product was dried at 60 °C for 12 h in a vacuum, and the sample obtained was a yellow color.

2.3. Synthesis of Phen-Functionalized SBA-15 Mesoporous Material (phen−SBA-15). The synthesis procedure was similar to our previous publication with some minor modification.[11] P123 (1.0 g) was dissolved in the deionized water (7.5 mL) and 2 M HCl solution (30 mL) at 35 °C. A mixture of TEOS and phen−Si was added into the solution, with the following molar composition: 0.04 phen−Si:1.0 TEOS:0.0172 P123:6 HCl:208.33 H_2O. The mixture was stirred at 35 °C for 24 h and transferred into a Teflon bottle sealed in an autoclave, which was then heated at 100 °C for 48 h. The solid product was collected by filtration, washed thoroughly using deionized water, and dried at 60 °C. Removal of copolymer surfactant P123 was conducted by Soxhlet extraction with ethanol heated under reflux for 24 h. The material obtained was dried at 60 °C for 12 h in a vacuum and showed a light-pink color.

2.4. Synthesis of the $Ln(dbm)_3(H_2O)_2$ Complex (Ln = Er, Yb, Nd). An appropriate amount of 1.0 M sodium hydroxide solution was added dropwise to Hdbm ethanol solution under stirring to adjust the pH value to approximately 7. The $LnCl_3$ ethanol solution was added dropwise into this mixture under stirring with the molar ratio of Ln^{3+}/Hdbm being 1:3. Then an appropriate amount of water was added, and the mixture was heated under reflux for 6 h and then cooled to room temperature. The precipitates were collected by filtration, washed with water and ethanol, and dried overnight at 70 °C under vacuum.

2.4.1. Elemental Analysis. For $Er(dbm)_3(H_2O)_2$, Calcd: C, 61.70%; H, 4.23%. Found: C, 61.51%; H, 4.41%. For $Nd(dbm)_3(H_2O)_2$, Calcd: C, 63.36%; H, 4.34%. Found: C,

63.49%; H, 4.59%. For $Yb(dbm)_3(H_2O)_2$, Calcd: C, 61.30%; H, 4.20%. Found: C, 61.53%; H, 4.01%.

2.5. Synthesis of MCM-41 Mesoporous Material Covalently Bonded with Er(dbm)$_3$phen Ternary Complex (Denoted as Er(dbm)$_3$phen−MCM-41$_{(X,Y)}$). The phen−MCM-41 was added to an $Er(dbm)_3(H_2O)_2$ ethanol solution under stirring with the following molar composition: $Er(dbm)_3(H_2O)_2$/phen−MCM-41 = *X*, where $X = 1, 2, 3, 5, 6, 7, 8, 10, 12, 13$, and 14. The mixture was heated under reflux for *Y* h ($Y = 3, 6, 12, 18$, and 24, respectively) and was recovered by filtration. Then the sample was soaked in an appropriate amount of acetone and heated under reflux for half an hour, followed by filtration and extensive washing with acetone to remove the excess of $Er(dbm)_3(H_2O)_2$. In the obtained material, the phen−Si acts as a bidentate ligand and expels two water molecules from the first coordination sphere of the $Er(dbm)_3(H_2O)_2$ complex. In this way, $Er(dbm)_3$phen is formed and the complex is attached to the MCM-41 mesoporous material. The resulting samples were dried at 60 °C under vacuum for 12 h and denoted as Er(dbm)$_3$phen−MCM-41$_{(X,Y)}$.

2.6. Synthesis of MCM-41 Mesoporous Material Covalently Bonded with Ln(dbm)$_3$phen Ternary Complex [Ln(dbm)$_3$phen−MCM-41, Ln = Er, Nd, Yb]. The material Ln(dbm)$_3$phen−MCM-41 (Ln = Er, Nd, Yb) was prepared according to the procedure of Er(dbm)$_3$phen−MCM-41$_{(X,Y)}$ ($X = 12$, $Y = 6$).

2.7. Synthesis of SBA-15 Mesoporous Material Covalently Bonded with Ln(dbm)$_3$phen Ternary Complex [Ln(dbm)$_3$phen−SBA-15, Ln = Er, Nd, Yb]. The synthesis procedure for Ln(dbm)$_3$phen−SBA-15 was similar to that of Ln(dbm)$_3$phen−MCM-41 except that phen−MCM-41 was replaced by phen−SBA-15.

2.8. Characterization. The CHN elemental analyses were carried out on a VarioEL analyzer. The Br elemental analysis was measured by titration. Small-angle X-ray diffraction patterns (XRD) were recorded with a Rigaku-Dmax 2500 diffractometer using Cu Kα radiation (40 kV, 200 mA) at a step width of 0.01°. FT-IR spectra were measured within a 4000−400 cm^{-1} region on an American BIO-RAD Company model FTS135 infrared spectrophotometer with the KBr pellet technique. Nitrogen (N_2) adsorption/desorption isotherms were measured by using a Nova l000 analyzer with nitrogen. The samples were outgassed for 4 h at 120 °C before the measurements. Surface areas were calculated by the Brunauer−Emmett−Teller (BET) method, and pore sizes by the Barrett−Joyner−Halenda (BJH) methods. The excitation and emission spectra of the solid-state samples were measured with an Edinburgh Analytical Instruments FLS920 equipped with the laser diode (LD) from the PicoQuant Company as the light source. The time-resolved measurement for Ln(dbm)$_3$phen−MCM-41 and Ln(dbm)$_3$phen−SBA-15 (Ln = Nd, Yb) was done on an Edinburgh Instruments FLS920 equipped with a 397 nm picosecond laser diode (LD) from the PicoQuant Company, and for Er(dbm)$_3$phen−MCM-41 and Er(dbm)$_3$phen−SBA-15 was done on an Edinburgh Instruments combined fluorescence lifetime and steady-state spectrometer FLS920 equipped with a μF900 lamp. The content of Ln^{3+} (Ln = Er, Nd, Yb) ion was obtained by inductively coupled plasma-atomic emission spectroscopy and mass spectroscopy (ICP-AES/MS) measurement with a TJA-POEMS spectrometer.

3. Results and Discussion

3.1. Parent Materials of phen−MCM-41 and phen−SBA-15 with the phen−Si/TEOS Ratio of 0.04. MCM-41[7] and SBA-15,[15] the mesoporous silica-walled materials with a regularly ordered two-dimensional (2D) hexagonal arrangements of cylindrical pores (space group *P6mm*), have a large potential as support materials due to their controlled pore size and a narrow pore-size distribution. MCM-41 silicas have pore sizes in the range of 2−6 nm and smooth pore surfaces, while SBA-15 silicas can be typically prepared in the range of 5−10 nm and exhibit considerable surface roughness, which is attributed to $(SiO_2)_n$ islands on the surface.[16] In recent years, various methods of functionalizing the surfaces of periodic mesoporous materials with organic groups have been widely investigated because surface modification permits tailoring of the surface properties for numerous potential applications.[17] In general, there are two approaches to surface modification, i.e., postsynthesis grafting and co-condensation.[18] The postsynthesis grafting method possesses several advantages, yet the main drawback of the method is that the distribution of the functional groups is not uniform and, even more unfortunately, difficult to control.[18c] The other method, co-condensation, allows modification of the surfaces of the mesoporous materials in a single step by copolymerization of organosilane with silica or organosilica precursors in the presence of a surfactant. This approach enables a higher and more homogeneous surface coverage of organosilane functionalities. In addition, the stability of the materials prepared by co-condensation is believed to be better than that of the postmodified materials.[17g]

In our case, because planar optical amplifiers have a smaller interaction length with respect to a NIR-lanthanide (Er^{3+}, Nd^{3+}) doped fiber amplifier, a higher ion concentration is required to obtain a sufficient optical gain. However, because of the concentration effect, high doping levels of lanthanide ion usually quench the fluorescence and accordingly reduce the performance of the amplifier. To reduce concentration quenching, the lanthanide ions should be dispersed uniformly at a molecular level.[19] Thus, the co-condensation method was selected to synthesize the phen−MCM-41 and phen−SBA-15 materials, following with the $Ln(dbm)_3(H_2O)_2$ introduced into these functionalized mesoporous materials through a ligand-exchange reaction. In addition, it is also important to understand the role of the phen−Si organosilane during the co-assembly process and its concentration effect on the pore structure. The increase in phen−Si concentration will result in the reduction of diffraction intensity or the disordered structure for phen−MCM-41 or phen−SBA-15 materials. The lower loading of functionality will be followed with a relatively decreasing amount of the lanthanide complexes linked to the functionalized frameworks. According to our previous report,[11a] an optimum molar ratio (phen−Si/TEOS = 0.04) can be employed to synthesize phen−SBA-15 with a high loading of functionality yet a good mesostructure. Therefore, the phen−Si-to-TEOS molar ratio of 0.04 is used in the initial mixture for the syntheses of phen−MCM-41 and phen−SBA-15 materials, respectively. The preservation of the chelate ligand structure (phen−Si) during the hydrothermal syntheses and the surfactant extraction processes for phen−MCM-41 and phen−SBA-15 materials was confirmed by Fourier transform infrared (FT-IR) and ^{29}Si MAS NMR spectroscopies, as we reported previously.[11]

X-ray diffraction patterns of the as-synthesized and surfactant-extracted phen−MCM-41 and surfactant-extracted phen−SBA-15 materials are presented in Figure 1. For the as-synthesized and surfactant-extracted phen−MCM-41 materials (Figure 1a), the patterns clearly show the order of the hexagonal array of the MCM-41 structure and exhibit a high-intensity (100) reflection and three higher-angle reflections that can be indexed for the (110), (200), and (210) reflections.[7] After the surfactant

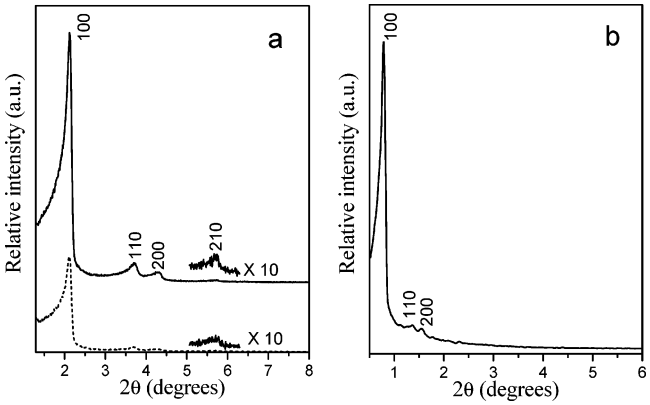

Figure 1. XRD patterns for (a) as-synthesized phen−MCM-41 (short dashed line) and surfactant-extracted phen−MCM-41 (solid line), and (b) surfactant-extracted phen−SBA-15.

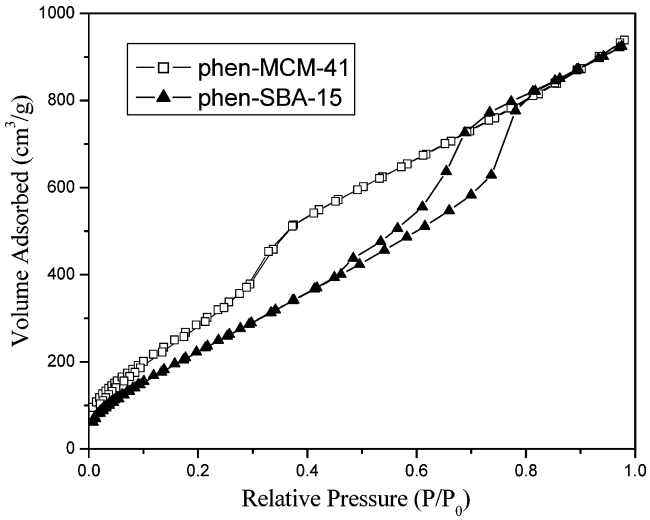

Figure 2. N_2 adsorption/desorption isotherms for surfactant-extracted phen−MCM-41 and phen−SBA-15.

was extracted, the diffraction intensities are found to increase due to the further cross-linking of silicates.[20] The surfactant-extracted phen−SBA-15 (Figure 1b) also exhibits well-resolved diffraction peaks that can be indexed to be (100), (110), and (200) diffractions, being typical of two-dimensional hexagonal (*P*6*mm*) SBA-15. The materials phen−MCM-41 and phen−SBA-15 under study show at least three Bragg peaks, which indicates that highly ordered materials of typical MCM-41 and SBA-15 structures were obtained.

The pore structures of these materials were further characterized by using the nitrogen sorption experiments. Figure 2 displays the nitrogen adsorption/desorption isotherms for the surfactant-extracted phen−MCM-41 and phen−SBA-15 materials. The isotherm of phen−MCM-41 shows a type IV isotherm, featuring a sharp increase of capillary condensation at relative pressure $P/P_0 \geq 0.27$. For phen−SBA-15, a type IV isotherm with a clear H1-type hysteresis that is typical of SBA-15 mesoporous materials is obtained.[15] In contrast to the nitrogen adsorption/desorption result for the phen−MCM-41 mesoporous material, the capillary condensation in the phen−SBA-15 product occurs at a higher relative pressure ($P/P_0 \sim 0.70$), suggesting larger pore sizes.[21] From the BET surface area and BJH pore diameter of the phen−MCM-41 and phen−SBA-15 materials (see Table 1), it is observed that these data are less than those typically reported for pure MCM-41 and SBA-15 silicas, respectively. This is attributed to the presence of the organic ligand on the pore surface.[22]

3.2. Er(dbm)$_3$phen-Functionalized MCM-41 Mesoporous Materials [Er(dbm)$_3$phen−MCM-41$_{(X,Y)}$]. We have synthesized a broad range of materials Er(dbm)$_3$phen−MCM-41$_{(X,Y)}$ with different characteristics by changing the synthesis parameters (the Er(dbm)$_3$(H$_2$O)$_2$/phen−MCM-41 molar ratio *X*, and the reaction time *Y*) in a controlled way. Concerning Er(dbm)$_3$phen−MCM-41$_{(X,Y)}$ ($X = 1$, 2, 3, 5, 6, 7, 8, 10, 12, 13, and 14, respectively, and $Y = 12$), i.e., Er(dbm)$_3$phen−MCM-41$_{(X,12)}$, all the synthesized materials exhibit very similar X-ray diffraction patterns, as illustrated by the representative patterns in Figure 3A. Compared with the phen−MCM-41 mesoporous material (curve a), the Er(dbm)$_3$phen−MCM-41$_{(X,12)}$ materials all show three well-resolved diffraction peaks that are characteristic of well-ordered hexagonal MCM-41. The representative N_2 adsorption/desorption isotherms of Er(dbm)$_3$phen−MCM-41$_{(X,12)}$ are depicted in Figure 3B. Upon the introduction of Er(dbm)$_3$(H$_2$O)$_2$ complex into the phen−MCM-41 mesoporous material, there is no change in the isotherm type (type IV), proving the conservation of the structural ordering of the MCM-41.

Chemical analysis of the Er^{3+} ion content in all Er(dbm)$_3$phen−MCM-41$_{(X,12)}$ materials shows that only a fraction of the Er(dbm)$_3$phen complexes have been covalently bonded with the MCM-41. Figure 4 depicts the relationship of *X* in the initial mixture to the Er^{3+} ion content of the Er(dbm)$_3$phen−MCM-41$_{(X,12)}$ materials. It seems that the Er^{3+} ion content in Er(dbm)$_3$phen−MCM-41$_{(X,12)}$ materials has an upper limit (within error of measurement), and after $X = 12$, the reaction reaches equilibrium. On the basis of the result above, we chose $X = 12$ and changed the reaction time *Y*, and obtained the corresponding materials Er(dbm)$_3$phen−MCM-41$_{(12,Y)}$ ($Y = 3$, 6, 12, 18, and 24 h, respectively). The elemental analysis results (Table 2) show that the Er^{3+} ion content has the maximum when the time *Y* is 6 h. The big drop of the Er ion content after 18 h was supposed to be the loss of the coordinated Er ion caused by the loss of the phen ligand during the excessive reaction time. In addition, the X-ray diffraction patterns and N_2 adsorption/desorption isotherms show that the Er(dbm)$_3$phen−MCM-41$_{(12,Y)}$ ($Y = 3$, 6, 12, 18, and 24 h, respectively) materials all exhibit the typical hexagonal feature of MCM-41 (not shown). Taking into account the results mentioned above and the similar chemistry characteristics (size and charge) of the trivalent lanthanide ions, $X = 12$ (namely Ln(dbm)$_3$(H$_2$O)$_2$/phen−MCM-41 molar ratio or Ln(dbm)$_3$(H$_2$O)$_2$/phen−SBA-15 molar ratio) and $Y = 6$ h were selected as the candidates for the following preparation of Ln(dbm)$_3$phen−MCM-41 and Ln(dbm)$_3$phen−SBA-15 (Ln = Er, Nd, Yb) materials.

3.3. Ln(dbm)$_3$phen−MCM-41 and Ln(dbm)$_3$phen−SBA-15 Materials (Ln = Er, Nd, Yb). *3.3.1. Structural Characterizations.* The powder XRD patterns of phen−MCM-41 and phen−SBA-15 before and after the introduction of Ln(dbm)$_3$(H$_2$O)$_2$ complex (Ln = Er, Nd, Yb) are shown in Figure 5 and Figure 6, respectively. All Ln(dbm)$_3$phen−MCM-41 and Ln(dbm)$_3$phen−SBA-15 materials exhibit XRD patterns typically observed for MCM-41 and SBA-15, respectively, consisting of a strong (100) reflection at a low angle and two small peaks (110, 200) at a higher angle. Compared with those of phen−MCM-41 and phen−SBA-15 materials (see Table 1), the d_{100} spacing values of Ln(dbm)$_3$phen−MCM-41 and Ln(dbm)$_3$phen−SBA-15 are nearly unchanged, respectively, indicating that their framework hexagonal ordering has been preserved well after the introduction of the Ln(dbm)$_3$(H$_2$O)$_2$ complex. It is also worth noting that the Ln(dbm)$_3$phen−MCM-41 and Ln(dbm)$_3$-

TABLE 1: Structural Parameters of Phen−MCM-41, Phen−SBA-15, Ln(dbm)$_3$phen−MCM-41, and Ln(dbm)$_3$phen−SBA-15 (Ln = Er, Nd, Yb)[a]

sample	d_{100} (nm)	a_0 (nm)	S_{BET} (m^2g^{-1})	V (cm^3g^{-1})	D (nm)	h_w (nm)
phen−MCM-41	3.96	4.57	1194	1.45	2.78	1.79
Er(dbm)$_3$phen−MCM-41	3.87	4.47	1142	1.25	2.56	1.91
Nd(dbm)$_3$phen−MCM-41	3.92	4.53	1149	1.24	2.56	1.97
Yb(dbm)$_3$phen−MCM-41	3.97	4.58	1114	1.19	2.57	2.01
phen−SBA-15	11.06	12.77	938.7	1.43	6.46	6.31
Er(dbm)$_3$phen−SBA-15	11.03	12.74	795.2	1.23	5.70	7.04
Nd(dbm)$_3$phen−SBA-15	10.92	12.61	779.4	1.21	5.73	6.88
Yb(dbm)$_3$phen−SBA-15	10.90	12.59	745.4	1.21	5.78	6.81

[a] d_{100} is the d(100) spacing, a_0 the cell parameter ($a_0 = 2d_{100}/\sqrt{3}$), S_{BET} the BET surface area, V the total pore volume, D the average pore diameter, and h_w the wall thickness, calculated by a_0-D.

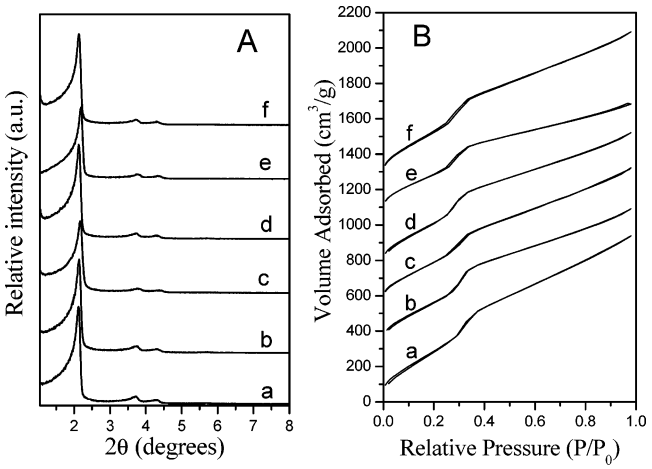

Figure 3. XRD patterns (A) and N_2 adsorption/desorption isotherms (B) of Er(dbm)$_3$phen−MCM-41$_{(X,12)}$ materials, when $X = 0$ (a), 1 (b), 3 (c), 8 (d), 12 (e), 14 (f). To allow a better comparison, the isotherms for $X = 1$, 3, 8, 12, and 14 materials were shifted by 300, 550, 750, 1050, and 1250 cm^3/g, respectively.

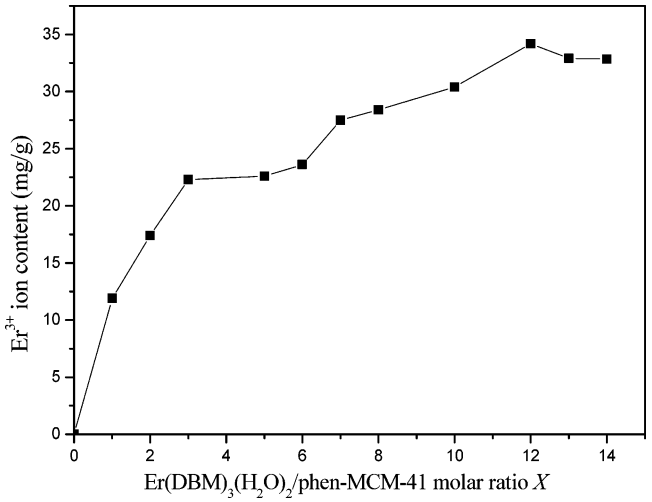

Figure 4. Relationship between the Er(dbm)$_3$(H_2O)$_2$/phen−MCM-41 molar ratio X in the initial mixture and the Er^{3+} ion content of the Er(dbm)$_3$phen−MCM-41$_{(X,12)}$ materials.

phen−SBA-15 materials exhibit decreased diffraction intensity as compared to the parent phen−MCM-41 and phen−SBA-15 materials, respectively (Figures 5 and 6). This is probably due to the presence of Ln(dbm)$_3$phen inside the pore channels of Ln(dbm)$_3$phen−MCM-41 and Ln(dbm)$_3$phen−SBA-15 materials, respectively.

Figures 7 and 8 depict the N_2 adsorption/desorption isotherms of Ln(dbm)$_3$phen−MCM-41 and Ln(dbm)$_3$phen−SBA-15 as well as their parent materials, respectively. The Ln(dbm)$_3$phen−

TABLE 2: Content of Er^{3+} Ion for the Er(dbm)$_3$phen−MCM-41$_{(12,Y)}$ Materials

Er(dbm)$_3$phen−MCM-41$_{(12,Y)}$	Er^{3+} ion content (mg/g)
$Y = 3$	28.8
$Y = 6$	37.3
$Y = 12$	34.2
$Y = 18$	25.1
$Y = 24$	26.5

MCM-41 and Ln(dbm)$_3$phen−SBA-15 materials all show similar isotherms to those of their parent materials phen−MCM-41 and phen−SBA-15, i.e., type IV isotherm, characteristic of mesoporous materials according to the IUPAC classification.[23] An H1 hysteresis loop is only observed for each Ln(dbm)$_3$phen−SBA-15 mesoporous material. This can be attributed to the fact that the occurrence of sorption hysteresis depends on temperature, pore size, and shape, i.e., the thermodynamic states of pore fluid and bulk fluid.[24] Thus, materials with cylindrical pores <4 nm do not show a hysteresis loop. The pore sizes were calculated from the desorption branch of the isotherms by using the Barrett−Joyner−Halenda (BJH) formula,[25] despite the fact that this well-established theory is actually valid only for materials with pores >4 nm and underestimates the diameter of mesopores with pore diameters <4 nm by approximately 1 nm.[26] However, it is an appropriate method for determining changes in the pore-size distributions. In addition, although more detailed and accurate calculations could be achieved by using the relatively new method that determines the pore sizes with the nonlocal density functional theory (NLDFT),[27] this model is so far only valid for pure porous structures, such as porous silicas, and not for host/guest systems in our case. So, for comparison reasons, the BJH-

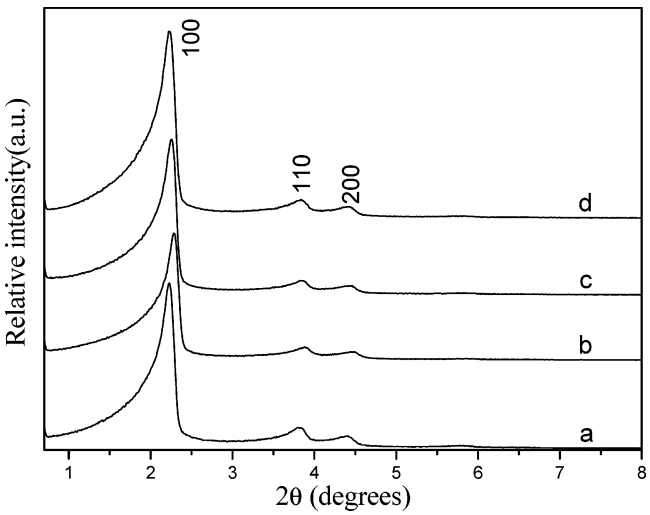

Figure 5. XRD patterns of phen−MCM-41 (a), and Ln(dbm)$_3$phen−MCM-41 when Ln = Er (b), Nd (c), and Yb (d).

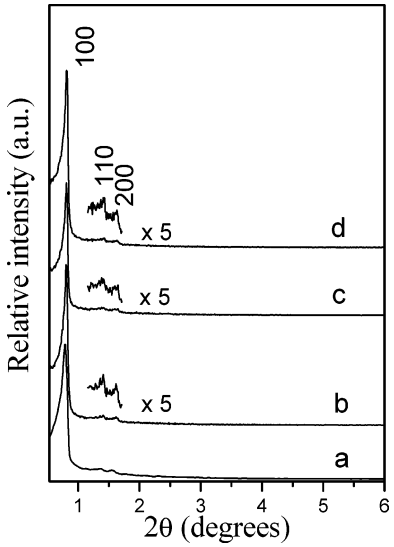

Figure 6. XRD patterns of phen−SBA-15 (a), and Ln(dbm)$_3$phen−SBA-15 when Ln = Er (b), Nd (c), and Yb (d).

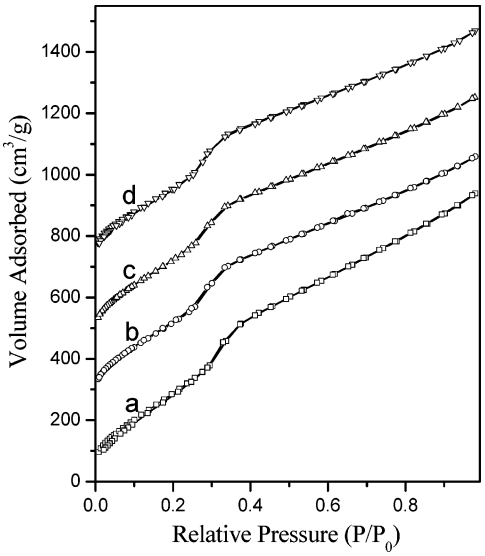

Figure 7. N_2 adsorption/desorption isotherms of phen−MCM-41 (a), and Ln(dbm)$_3$phen−MCM-41 when Ln = Er (b), Nd (c), and Yb (d). To allow a better comparison, the isotherms for Ln = Er, Nd, and Yb materials were shifted by 250, 450, and 700 cm^3/g, respectively.

algorithm was used for all materials in this work. The structure data of all these mesoporous materials (BET surface area, total pore volume, and pore size, etc.) were summarized in Table 1. It is shown that the surface area, pore volume, and pore size of the Ln(dbm)$_3$phen−MCM-41 and Ln(dbm)$_3$phen−SBA-15, as expected, decrease after introducing the Ln(dbm)$_3$(H_2O)$_2$ complexes into the phen−MCM-41 and phen−SBA-15, which is consistent with the presence of anchored Ln(dbm)$_3$phen in the Ln(dbm)$_3$phen−MCM-41 and Ln(dbm)$_3$phen−SBA-15.

3.3.2. Photoluminescence Studies. Figure 9 presents the excitation and emission spectra of Er(dbm)$_3$phen−MCM-41 and Er(dbm)$_3$phen−SBA-15 materials. For the two excitation spectra, they all show a broad band ranging from 250 to 445 nm, which is due to the absorption of the organic ligands. Compared with the pure Er(dbm)$_3$phen complex,[2a] the two excitation spectra become narrower and the maximum excitation wavelength shift from 415 to 386 and 397 nm for Er(dbm)$_3$phen−MCM-41 and Er(dbm)$_3$phen−SBA-15, respectively. The blue-shift of the excitation bands as the introduction of the erbium complex into the mesoporous materials was attributed to a

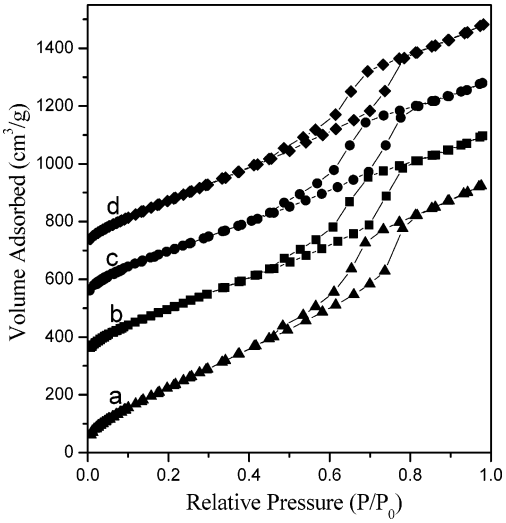

Figure 8. N_2 adsorption/desorption isotherms of phen−SBA-15 (a), and Ln(dbm)$_3$phen−SBA-15 when Ln = Er (b), Nd (c), and Yb (d). To allow a better comparison, the isotherms for Ln = Er, Nd, and Yb materials were shifted by 300, 500, and 700 cm^3/g, respectively.

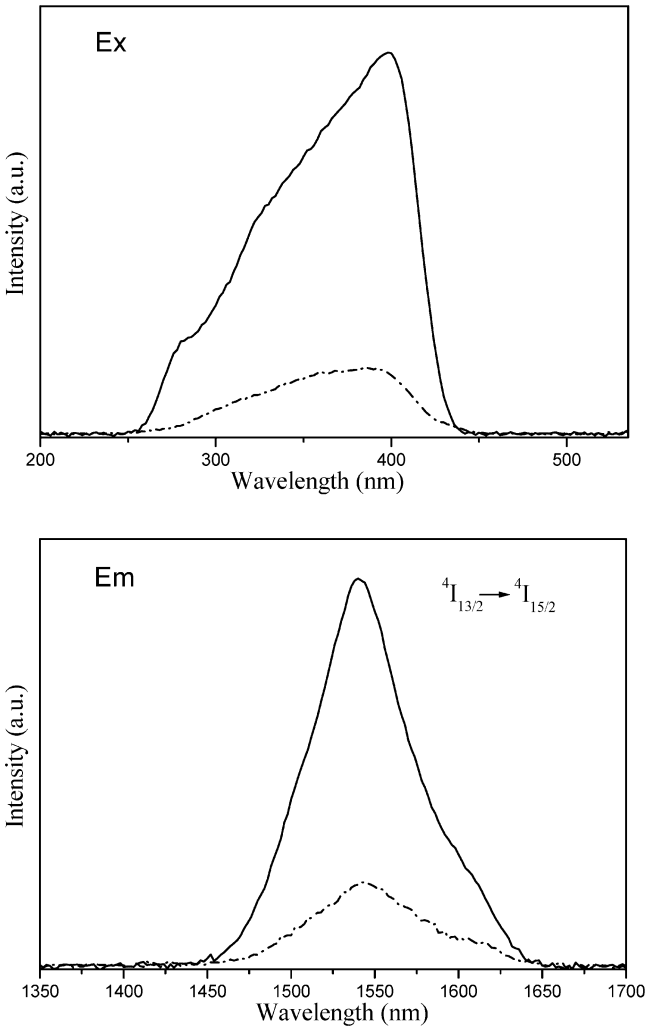

Figure 9. Excitation (λ_{em} = 1541 nm) and emission (λ_{ex} = 397 nm) spectra for Er(dbm)$_3$phen−MCM-41 (dash−dotted line) and Er(dbm)$_3$phen−SBA-15 (solid line).

hypsochromic effect resulting from the change in the polarity of the environment surrounding the erbium complex in the mesoporous materials.[11a] For the excitation spectrum of pure Er(dbm)$_3$phen complex,[2a] some small peaks, originating from

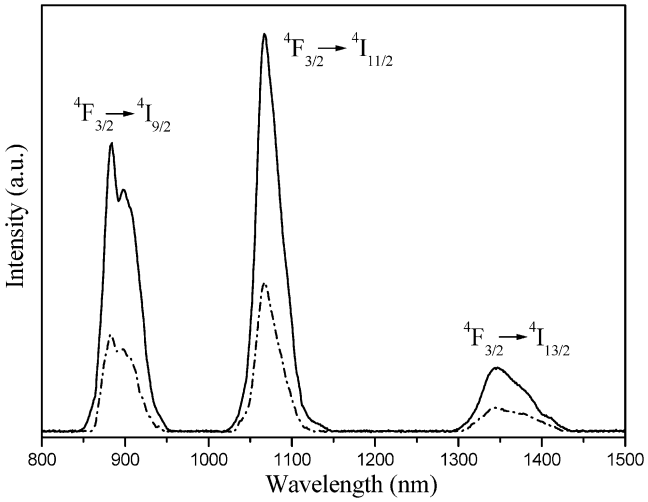

Figure 10. Emission spectra (λ_{ex} = 397 nm) for Nd(dbm)$_3$phen−MCM-41 (dash−dotted line) and Nd(dbm)$_3$phen−SBA-15 (solid line).

f−*f* absorption transitions of the Er^{3+} ion, are observed, yet no *f*−*f* transition of the Er^{3+} ion could be observed in the excitation spectra of Er(dbm)$_3$phen−MCM-41 and Er(dbm)$_3$phen−SBA-15, respectively. This indicates that the energy transfer from the ligands to the Er^{3+} ion is more efficient in Er(dbm)$_3$phen−MCM-41 and Er(dbm)$_3$phen−SBA-15 than in the pure Er(dbm)$_3$phen complex, an improvement of the Er^{3+} ion-sensitized process.[12f] After ligand-mediated excitation at 397 nm, the emission spectra of the Er(dbm)$_3$phen−MCM-41 and Er(dbm)$_3$phen−SBA-15 clearly show the emission bands centered at 1544 and 1540 nm, respectively. The emission bands cover large spectra range and extend from 1434 to 1664 nm and from 1430 to 1664 nm for Er(dbm)$_3$phen−MCM-41 and Er(dbm)$_3$phen−SBA-15, respectively, which are attributed to the transition from the first excited state ($^4I_{13/2}$) to the ground state ($^4I_{15/2}$) of the Er^{3+} ion. Recently, erbium-doped materials have attracted considerable attention in optical amplification because the transition around 1540 nm is in the right position of the third telecommunication window. To enable a wide gain bandwidth for optical amplification, a broad emission band is desirable.[2d,e] The full width at half-maximum (fwhm) of the $^4I_{13/2} \rightarrow {}^4I_{15/2}$ transition for the Er(dbm)$_3$phen−MCM-41 material is 76 nm, and the fwhm for Er(dbm)$_3$phen−SBA-15 is 72 nm. Such broad spectra enable a wide gain bandwidth for optical amplification. Therefore, the luminescent mesoporous materials can be potential candidates in polymeric erbium-doped optical amplifiers or planar waveguides.

The excitation spectra of Ln(dbm)$_3$phen−MCM-41 and Ln(dbm)$_3$phen−SBA-15 (Ln = Nd, Yb) are similar to those of Er(dbm)$_3$phen−MCM-41 and Er(dbm)$_3$phen−SBA-15, respectively, and also show broad bands due to the absorption of the organic ligands. Excitation of the ligands absorption bands at 397 nm resulted in the emission spectra of Nd(dbm)$_3$phen−MCM-41 and Nd(dbm)$_3$phen−SBA-15 (Figure 10), respectively. In the two curves, both of the luminescence spectra consist of three bands centered at λ = 883, 1067, and 1344 nm, which are attributed to the *f*−*f* transitions of $^4F_{3/2}$ (emitting level) → $^4I_{9/2}$, $^4F_{3/2} \rightarrow {}^4I_{11/2}$ and $^4F_{3/2} \rightarrow {}^4I_{13/2}$, respectively. The relative intensity sequence of these three transitions is I($^4F_{3/2} \rightarrow {}^4I_{11/2}$) > I($^4F_{3/2} \rightarrow {}^4I_{9/2}$) > I($^4F_{3/2} \rightarrow {}^4I_{13/2}$). Among the three bands of the emission spectra, the intensity of the transition at 1067 nm is the strongest, and for a long time this center has been found to have potential application in laser systems. The 1344 nm emission bands of the mesoporous materials offer the opportunity to develop new materials suitable for the optical amplifiers operating at 1.3 μm, one of the telecommunication windows.[28]

The emission spectra of Yb(dbm)$_3$phen−MCM-41 and Yb(dbm)$_3$phen−SBA-15 upon excitation at 397 nm are shown in Figure 10, respectively. In both curves, the prominent 980 nm emission band can be observed, which is assigned to the $^2F_{5/2} \rightarrow {}^2F_{7/2}$ transition of the Yb^{3+} ion. It should also be noted that the Yb^{3+} ion emission band is not a single sharp band, but an envelope of bands arising at the lower energy side than the primary 980 nm band. Similar splitting has been reported previously.[5a,6a,29] This may be the result of splitting of the energy levels of the Yb^{3+} ion as a consequence of ligand field effects.[2d] The Yb^{3+} ion has some advantages for laser emission due to its very simple energy level scheme, consisting of only two levels: the $^2F_{7/2}$ ground state and the $^2F_{5/2}$ excited state. The relatively broad absorption (with a relatively high absorption coefficient) is well suited for laser diode pumping in this range, and the smaller Stokes shift (about 650 cm^{-1}) between absorption and emission reduces the thermal loading of the material during laser operation.[30] The obtained high-intensity emission of the Yb^{3+} ion make these mesoporous materials very important to various photonic applications in ionic crystals and glasses. In addition, the relative transparency of human tissue at approximately 1000 nm suggests that in vivo luminescent probes operating at this wavelength (Yb-based emission) could have diagnostic value.[1]

The emission features of the Ln(dbm)$_3$phen−MCM-41 and Ln(dbm)$_3$phen−SBA-15 materials are similar to those found for the corresponding pure Ln(dbm)$_3$phen complexes,[2a,29c] suggesting that the Ln^{3+} ion is mostly present as Ln(dbm)$_3$phen, which is covalently linked to the parent mesoporous materials (Ln = Er, Nd, Yb).[11a,12f] As described above, we obtained the characteristic Ln^{3+} ion emission upon excitation at the absorption of the organic ligands in both Ln(dbm)$_3$phen−MCM-41 and Ln(dbm)$_3$phen−SBA-15 materials. The NIR luminescence obtained in this study shows that the ligands shield the lanthanide ions well from their surroundings and efficiently transfer energy from their triplet states to the Ln^{3+} ions. This is further evidence that ternary complex Ln(dbm)$_3$phen is covalently bonded to the network of MCM-41 and SBA-15 materials. The luminescence lifetimes (see Table 3) of the different lanthanide complexes bonded to the mesoporous materials were measured at room temperature by using an excitation wavelength of 397 nm and monitored around the most intense emission line (at 1541 nm for the Er^{3+} ion, at 1067 nm for the Nd^{3+} ion, and at 980 nm for the Yb^{3+} ion). All the data are well fitted by a single-exponential function, confirming that all lanthanide ions occupy the same average local environment within each sample.[12f] The lower values were observed for Ln(dbm)$_3$phen−MCM-41 compared to those of corresponding Ln(dbm)$_3$phen−SBA-15 materials. This may be attributed to the fact that the nonradiative (k_{nr}) transition probability is higher in Ln(dbm)$_3$phen−MCM-41, despite the similar first-coordination shells of lanthanide ion to those of Ln(dbm)$_3$-phen−SBA-15.

The elemental analyses of Ln ions (Ln = Er, Nd, Yb) of the Ln(dbm)$_3$phen−MCM-41 and Ln(dbm)$_3$phen−SBA-15 materials are presented in Table 3. It can be seen that the Ln(dbm)$_3$phen−SBA-15 materials all show some decrease in the lanthanide ion content compared to the Ln(dbm)$_3$phen−MCM-41 materials, as indicated by the ion content for the Er^{3+}, Nd^{3+}, and Yb^{3+} ions, respectively. To evaluate the quantity of the phen groups in the phen−MCM-41 and phen−SBA-15 materials before the introduction of the Ln(dbm)$_3$(H_2O)$_2$ com-

TABLE 3: Elemental Analyses and Photoluminescent Data of Ln(dbm)$_3$phen−MCM-41 and Ln(dbm)$_3$phen−SBA-15 Materials[a]

	Ln(dbm)$_3$phen−MCM-41			Ln(dbm)$_3$phen−SBA-15		
sample	Ln = Er	Ln = Nd	Ln = Yb	Ln = Er	Ln = Nd	Ln = Yb
C_{Ln} (mmol/g)	0.223	0.266	0.179	0.118	0.134	0.103
C_{Ln} (mol %)	1.80	2.27	1.35	0.82	0.95	0.70
I_{Ln}	1.187×10^6	6.593×10^5	2.414×10^6	5.185×10^6	1.917×10^6	4.928×10^6
I_{Ln}/C_{Ln}	6.59×10^5	2.90×10^5	17.9×10^5	63.2×10^5	20.2×10^5	70.4×10^5
τ (μs)	2.29	0.23	12.1	2.40	0.28	12.3

[a] The contents of the Ln ions in molar percentage [C_{Ln} (mol %)]. The emission intensities of the $^4I_{13/2} \rightarrow {}^4I_{15/2}$ transition for Ln = Er (I_{Er}), the $^4F_{3/2} \rightarrow {}^4I_{11/2}$ transition for Ln = Nd (I_{Nd}), and the $^2F_{5/2} \rightarrow {}^2F_{7/2}$ transition for Ln = Yb (I_{Yb}). The emission intensity divided by the contents of the Ln ions in molar percentage (I_{Ln}/C_{Ln}). The luminescence lifetimes (τ).

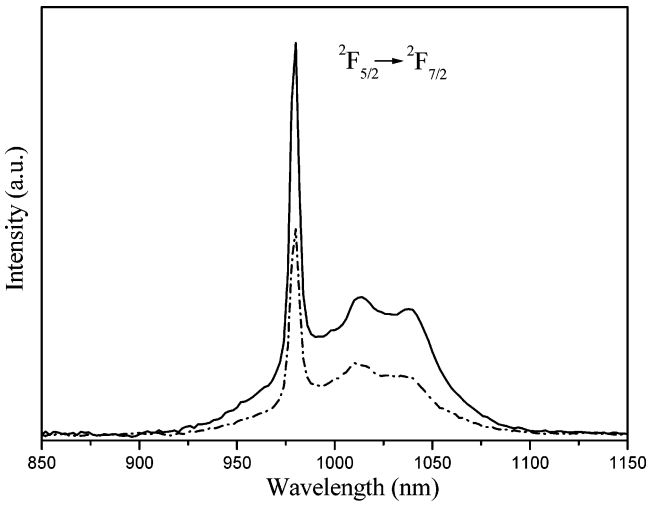

Figure 11. Emission spectra (λ_{ex} = 397 nm) for Yb(dbm)$_3$phen−MCM-41 (dash−dotted line) and Yb(dbm)$_3$phen−SBA-15 (solid line).

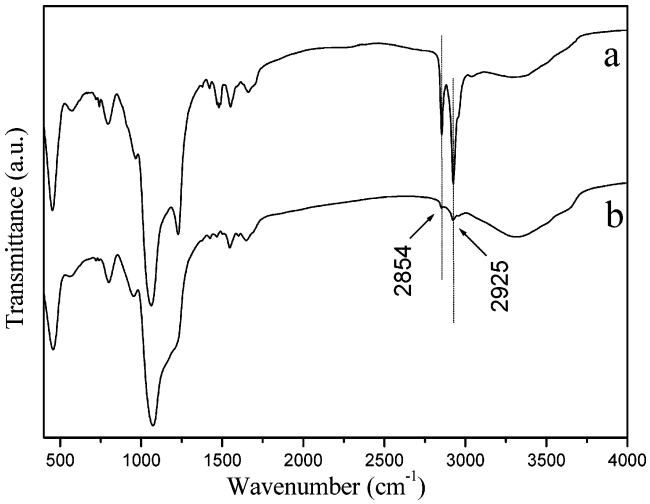

Figure 12. FT-IR spectra for as-synthesized phen−MCM-41 (a), and surfactant-extracted phen−MCM-41 (b).

plexes, the N elemental analysis has been utilized to characterize the parent phen−MCM-41 and phen−SBA-15 materials. However, CTAB, the surfactant used for the synthesis of phen−MCM-41, also has the element N. And from the IR spectra (see Figure 12), the surfactant-extracted phen−MCM-41 exhibits very weak ν(C−H) vibrations in the region of 2700−3000 cm^{-1}, which confirms the removal of most of the surfactant CTAB, but still incomplete. So the Br elemental analysis was performed on the surfactant-extracted phen−MCM-41 (Table 4). As shown in Table 4, the total amount of N in phen−MCM-41 is 1.933 mmol/g, yet there is 0.207 mmol/g from the CTAB. Thus, the amounts of phen−Si are 0.345 and 0.365 mmol/g for phen−MCM-41 and phen−SBA-15, respectively. Interestingly, phen−SBA-15 gives a higher phen group quantity than the phen−MCM-41 does, yet the Ln(dbm)$_3$phen−SBA-15 has the lower lanthanide ion content after the introduction of the Ln(dbm)$_3$(H$_2$O)$_2$ complexes (Ln = Er, Nd, Yb). It is well-known that the porous structure of SBA-15, different from that of MCM-41, consists not only of large, uniform, and ordered mesopores, but also of much smaller complementary micropores that provide connectivity between the ordered mesopores.[31] The formation of micropores in the silica walls might be explained by the penetration of hydrophilic poly(ethyleneoxide) chains of the triblock copolymer in the silica wall. According to the reference,[31a,b] we, therefore, assume that the phen−SBA-15 prepared through the co-condensation method, consists of cylindrical mesopores that are interconnected by micropores in the pore walls (Scheme 1). The micropores might be too small to be accessible for the Ln(dbm)$_3$(H$_2$O)$_2$ (around 1.6 nm) complexes, or some phen−Si groups might block the pore mouth of the micropores. As a consequence, those micropores of phen−SBA-15 are not accessible for Ln(dbm)$_3$-(H$_2$O)$_2$ complexes, resulting in a large reduction of the lanthanide ion content (Table 3).

TABLE 4: Contents of N, Br, and Organic Components for Mesoporous Phen−MCM-41 and Phen−SBA-15[a]

materials	N_{total} (mmol/g)	Br (mmol/g)	$N_{phen-Si}$ (mmol/g)	phen−Si (mmol/g)
phen−MCM-41	1.933	0.207	1.726	0.345
phen−SBA-15	1.824		1.824	0.365

[a] N_{total} is the total content of N element, $N_{phen-Si}$ the content of N element from phen−Si.

However, the Ln(dbm)$_3$phen−SBA-15 presents the higher intensity and the longer lifetime of NIR luminescence (see Figures 9, 10, and 11, Table 3) despite the lower lanthanide ion content as compared to that of Ln(dbm)$_3$phen−MCM-41 (Ln = Er, Nd, Yb). The luminescence behavior of the ternary complexes functionalized mesoporous materials (Ln(dbm)$_3$phen−MCM-41 and Ln(dbm)$_3$phen−SBA-15) may depend on the lanthanide ion content and on the mesoporous structure of the materials. A possible explanation for this difference is the self-quenching effect: because of the relatively small pore size and higher lanthanide ion loading, local lanthanide concentration of the Ln(dbm)$_3$phen−MCM-41 materials may be higher than the average concentration calculated. Because of the local high concentration, energy transfer from one Ln^{3+} ion to another can occur and the photon can migrate among these clustered regions, followed by quenching at a defect site in the Ln(dbm)$_3$phen−MCM-41 materials.[32] Besides, the amount of phen groups are 0.345 and 0.365 mmol/g for the parent phen−MCM-41 and phen−SBA-15 materials (Table 4), respectively. By taking into account the BET specific surface area, the surface coverage can be estimated as 0.17 and 0.23 phen molecules per nm^2 in the parent phen−MCM-41 and phen−SBA-15 materials, respectively. That is, there are more residual surface silanols that were

SCHEME 1: Schematic Representation of Ln(dbm)$_3$phen−SBA-15 Structure Where the Micropores Are Not Accessible for Ln(dbm)$_3$(H$_2$O)$_2$ Complexes (Ln = Er, Nd, Yb)

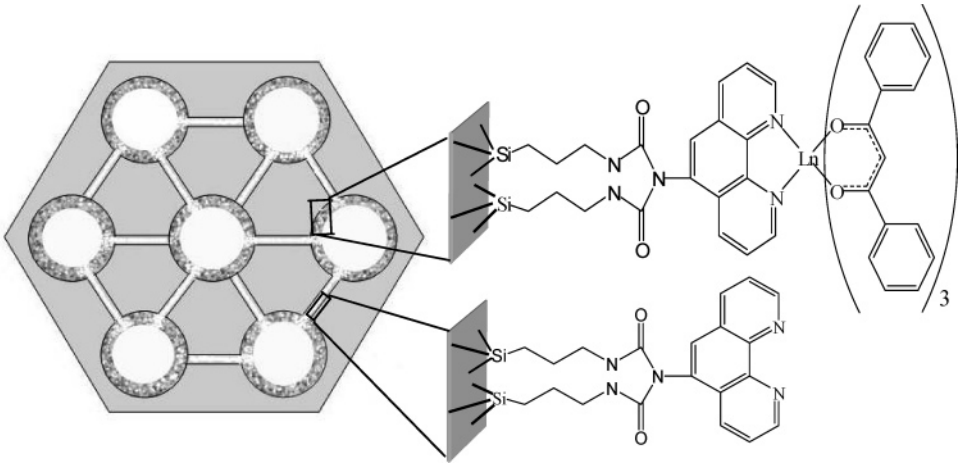

unfunctionalized with the organic phen−Si groups in the phen−MCM-41 material, which results in a substantial increase of the nonradiative multiphonon decay as caused by the stretching vibration of the −OH groups.[12f,33] As a result, the photoluminescence intensity will be lower and the luminescence lifetime shorter for the Ln(dbm)$_3$phen−MCM-41 materials (Ln = Er, Nd, Yb). The relative luminescent intensities (integrated intensities) of the $^4I_{13/2} \rightarrow {}^4I_{15/2}$ transition for Ln = Er (I_{Er}), the $^4F_{3/2} \rightarrow {}^4I_{11/2}$ transition for Ln = Nd (I_{Nd}), and the $^2F_{5/2} \rightarrow {}^2F_{7/2}$ transition for Ln = Yb (I_{Yb}) of the Ln(dbm)$_3$phen−MCM-41 and Ln(dbm)$_3$phen−SBA-15 materials are listed in Table 3. As mentioned above, the I_{Ln} of Ln(dbm)$_3$phen−SBA-15 are all higher than those of Ln(dbm)$_3$phen−MCM-41. When the luminescent intensity I_{Ln} is divided by the content of the Ln^{3+} ion C_{Ln}, the I_{Ln}/C_{Ln} of Ln(dbm)$_3$phen−SBA-15 is almost 10 times higher than that of Ln(dbm)$_3$phen−MCM-41 (Ln = Er, Nd, Yb). This behavior shows that, on the basis of $X = 12$ and $Y = 6$, the phen−SBA-15 mesoporous material is somewhat superior to phen−MCM-41 as the parent of NIR-luminescence lanthanide complexes.

4. Conclusions

In the present work, through the systematic and comparative study of the Er(dbm)$_3$phen−MCM-41$_{(X,Y)}$ mesoporous materials, the synthesis parameters $X = 12$ and $Y = 6$ were selected as the candidate conditions. On the basis of these conditions, the Ln(dbm)$_3$phen complexes have been covalently immobilized in the ordered mesoporous materials MCM-41 and SBA-15 via a functionalized phen group, and the obtained Ln(dbm)$_3$phen−MCM-41 and Ln(dbm)$_3$phen−SBA-15 materials all retain their mesoscopically ordered structures. After ligand-mediated excitation, the emission spectra of the Ln(dbm)$_3$phen−MCM-41 and Ln(dbm)$_3$phen−SBA-15 materials all show the characteristic NIR luminescence of the corresponding lanthanide ions through the intramolecular energy transfer from the ligands to the lanthanide ions. These luminescent mesoporous materials could have potential applications in optical amplifiers (operating at 1.3 or 1.5 μm), laser systems, or medical diagnostics. In addition, in a comparison of the luminescence behavior for the Ln(dbm)$_3$phen−MCM-41 and Ln(dbm)$_3$phen−SBA-15 materials, it is observed that the SBA-15-supported materials show an overall increase in relative luminescent intensity and lifetime compared to the MCM-41-supported materials, which was investigated by the comparison of the lanthanide ion content and the pore structures of the two kinds of materials. Since various lanthanide complexes and pore materials are now available, we believe that it is feasible to obtain various NIR-luminescent mesoporous materials. The ability that the mesostructured materials will retain their structures and properties after being covalently bonded with a number of NIR-luminescent lanthanide complexes opens the field to ordered multicomposite materials for lasers and optical amplification applications.

Acknowledgment. This work was supported by the National Natural Science Foundation of China (grant nos. 20372060, 20131010, 20490210, 20340420326), the "863" National Foundation for High Technology Development and Program (grant nos. 2002AA302105, 2002AA324080), and the National Basic Research Program of China ("973" Program) (grant no. 2006CB601103). We are grateful to Dr. E. Ma and Prof. J. G. Mao of the Fujian Institute of Research on the Structure of Matter, Chinese Academy of Sciences, for assistance with the fluorescence measurements.

References and Notes

(1) Davies, G. M.; Aarons, R. J.; Motson, G. R.; Jeffery, J. C.; Adams, H.; Faulkner, S.; Ward, M. D. *J. Chem. Soc., Dalton Trans.* **2004**, 1136.

(2) (a) Sun, L. N.; Zhang, H. J.; Fu, L. S.; Liu, F. Y.; Meng, Q. G.; Peng, C. Y.; Yu, J. B. *Adv. Funct. Mater.* **2005**, *15*, 1041. (b) Yanagida, S.; Hasegawa, Y.; Murakoshi, K.; Wada, Y.; Nakashima, N.; Yamanaka, T. *Coord. Chem. Rev.* **1998,** *171*, 461. (c) Park, O. H.; Seo, S. Y.; Bae, B. S.; Shin, J. H. *Appl. Phys. Lett.* **2003**, *82*, 2787. (d) Wolbers, M. P. O.; van Veggel, F. C. J. M.; Snellink-Ruël, B. H. M.; Hofstraat, J. W.; Geurts, F. A. J.; Reinhoudt, D. N. *J. Chem. Soc., Perkin Trans. 2* **1998**, 2141. (e) Van Deun, R.; Nockemann, P.; Görller-Walrand, C.; Binnemans, K. *Chem. Phys. Lett.* **2004,** *397*, 447.

(3) (a) Weissman, S. I. *J. Chem. Phys.* **1942**, *10*, 214. (b) Bekiari, V.; Lianos, P. *Adv. Mater.* **1998**, *10*, 1455. (c) Carlos, L. D.; Sá Ferreira, R. A.; Rainho, J. P.; de Zea Bermudez, V. *Adv. Funct. Mater.* **2002**, *12*, 819.

(4) (a) Driesen, K.; Van Deun, R.; Görller-Walrand, C.; Binnemans, K. *Chem. Mater.* **2004**, *16*, 1531. (b) Binnemans, K.; Lenaerts, P.; Driesen, K.; Görller-Walrand, C. *J. Mater. Chem.* **2004**, *14*, 191. (c) Klonkowski, A. M.; Lis, S.; Pietraszkiewicz, M.; Hnatejko, Z.; Czarnobaj, K.; Elbanowski, M. *Chem. Mater.* **2003**, *15*, 656. (d) Sanchez, C.; Lebeau, B.; Chaput, F.; Boilot, J. P. *Adv. Mater.* **2003**, *15*, 1969. (e) Sendor, D.; Kynast, U. *Adv. Mater.* **2002**, *14*, 1570.

(5) (a) Lenaerts, P.; Driesen, K.; Van Deun, R.; Binnemans, K. *Chem. Mater.* **2005**, *17*, 2148. (b) Kuriki, K.; Koike, Y.; Okamoto, Y. *Chem. Rev.* **2002**, *102*, 2347. (c) Yang, C. Y.; Srdanov, V.; Robinson, M. R.; Bazan, G. C.; Heeger, A. J. *Adv. Mater.* **2002**, *14*, 980.

(6) (a) Van Deun, R.; Moors, D.; De Fré, B.; Binnemans, K. *J. Mater. Chem.* **2003**, *13*, 1520. (b) Binnemans, K.; Görller-Walrand, C. *Chem. Rev.* **2002**, *102*, 2303.

(7) (a) Kresge, C. T.; Leonowicz, M. E.; Roth, W. J.; Vartuli, J. C.; Beck, J. S. *Nature* **1992**, *359*, 710. (b) Beck, J. S.; Vartuli, J. C.; Roth, W. J.; Leonowicz, M. E.; Kresge, C. T.; Schmitt, K. D.; Chu, C. T-W.; Olson,

D. H.; Sheppard, E. W.; McCullen, S. B.; Higgins, J. B.; Schlenker, J. L. *J. Am. Chem. Soc.* **1992**, *114*, 10834.

(8) (a) Davis, M. E. *Nature* **2002**, *417*, 813. (b) De Vos, D. E.; Dams, M.; Sels, B. F.; Jacobs, P. A. *Chem. Rev.* **2002**, *102*, 3615. (c) Scott, B. J.; Wirnsberger, G.; Stucky, G. D. *Chem. Mater.* **2001**, *13*, 3140. (d) Stein, A. *Adv. Mater.* **2003**, *15*, 763.

(9) (a) Meng, Q. G.; Boutinaud, P.; Franville, A.-C.; Zhang, H. J.; Mahiou, R. *Microporous Mesoporous Mater.* **2003**, *65*, 127. (b) Xu, Q. H.; Li, L. S.; Liu, X. S.; Xu, R. R. *Chem. Mater.* **2002**, *14*, 549. (c) Bartl, M. H.; Scott, B. J.; Huang, H. C.; Wirnsberger, G.; Popitsch, A.; Chmelka, B. F.; Stucky, G. D. *Chem. Commun.* **2002**, 2474.

(10) Li, H. R.; Lin, J.; Fu, L. S.; Guo, J. F.; Meng, Q. G.; Liu, F. Y.; Zhang, H. J. *Microporous Mesoporous Mater.* **2002**, *55*, 103.

(11) (a) Peng, C. Y.; Zhang, H. J.; Yu, J. B.; Meng, Q. G.; Fu, L. S.; Li, H. R.; Sun, L. N.; Guo, X. M. *J. Phys. Chem. B* **2005**, *109*, 15278. (b) Peng, C. Y.; Zhang, H. J.; Meng, Q. G.; Li, H. R.; Yu, J. B.; Guo, J. F.; Sun, L. N.; *Inorg. Chem. Commun.* **2005**, *8*, 440.

(12) (a) Li, H. R.; Lin, J.; Zhang, H. J.; Li, H. C.; Fu, L. S.; Meng, Q. G. *Chem. Commun.* **2001**, 1212. (b) Li, H. R.; Lin, J.; Zhang, H. J.; Fu, L. S.; Meng, Q. G.; Wang, S. B. *Chem. Mater.* **2002**, *14*, 3651. (c) Li, H. R.; Fu, L. S.; Lin, J.; Zhang, H. J. *Thin Solid Films* **2002**, *416*, 197. (d) Liu, F. Y.; Fu, L. S.; Wang, J.; Meng, Q. G.; Li, H. R.; Guo, J. F.; Zhang, H. J. *New J. Chem.* **2003**, *27*, 233. (e) Dong, D. W.; Jiang, S. C.; Men, Y. F.; Ji, X. L.; Jiang, B. Z. *Adv. Mater.* **2000**, *12*, 646. (f) Gago, S.; Fernandes, J. A.; Rainho, J. P.; Sá Ferreira, R. A.; Pillinger, M.; Valente, A. A.; Santos, T. M.; Carlos, L. D.; Ribeiro-Claro, P. J. A.; Gonçalves, I. S. *Chem. Mater.* **2005**, *17*, 5077. (g) Franville, A. C.; Zambon, D.; Mahiou, R. *Chem. Mater.* **2000**, *12*, 428.

(13) Lenaerts, P.; Storms, A.; Mullens, J.; D'Haen, J.; Görller-Walrand, C.; Binnemans, K.; Driesen, K. *Chem. Mater.* **2005**, *17*, 5194.

(14) Lecomte, J.-P.; Mesmaeker, A. K. D.; Demeunynck, M.; Lhomme, J. *J. Chem. Soc., Faraday Trans.* **1993**, *89*, 3261.

(15) (a) Zhao, D. Y.; Huo, Q. S.; Feng, J. L.; Chmelka, B. F.; Stucky, G. D. *J. Am. Chem. Soc.* **1998**, *120*, 6024. (b) Zhao, D. Y.; Feng, J. L.; Huo, Q. S.; Melosh, N.; Fredrickson, G. H.; Chmelka, B. F.; Stucky, G. D. *Science* **1998**, *279*, 548.

(16) Shenderovich, I. G.; Buntkowsky, G.; Schreiber, A.; Gedat, E.; Sharif, S.; Albrecht, J.; Golubev, N. S.; Findenegg, G. H.; Limbach, H. H. *J. Phys. Chem. B* **2003**, *107*, 11924.

(17) (a) Lim, M. H.; Blanford, C. F.; Stein, A. *J. Am. Chem. Soc.* **1997**, *119*, 4090. (b) Lim, M. H.; Blanford, C. F.; Stein, A. *Chem. Mater.* **1998**, *10*, 467. (c) Mercier, L.; Pinnavaia, T. J. *Adv. Mater.* **1997**, *9*, 500. (d) Meziani, M. J.; Zajac, J.; Jones, D. J.; Rozière, J.; Partyka, S. *Langmuir* **1997**, *13*, 5409. (e) Díaz, J. F.; Balkus, K. J., Jr.; Bedioui, F.; Kurshev, V.; Kevan, L. *Chem. Mater.* **1997**, *9*, 61. (f) Corriu, R. J. P.; Mehdi, A.; Reyé, C.; Thieuleux, C.; Frenkel, A.; Gibaud, A. *New J. Chem.* **2004**, *28*, 156. (g) Chong, A. S. M.; Zhao, X. S.; *J. Phys. Chem. B* **2003**, *107*, 12650.

(18) (a) Lim, M. H.; Stein, A. *Chem. Mater.* **1999**, *11*, 3285. (b) Yokoi, T.; Yoshitake, H.; Tatsumi, T. *J. Mater. Chem.* **2004**, *14*, 951. (c) Zhang, W. H.; Lu, X. B.; Xiu, J. H.; Hua, Z. L.; Zhang, L. X.; Robertson, M.; Shi, J. L.; Yan, D. S.; Holmes, J. D. *Adv. Funct. Mater.* **2004**, *14*, 544.

(19) Park, O. H.; Seo, S. Y.; Jung, J. I.; Bae, J. Y.; Bae, B. S. *J. Mater. Res.* **2003**, *18*, 1039.

(20) Hukkamäki, J.; Suvanto, S.; Suvanto, M.; Pakkanen, T. T. *Langmuir* **2004**, *20*, 10288.

(21) Jarupatrakorn, J.; Tilley, T. D. *J. Am. Chem. Soc.* **2002**, *124*, 8380.

(22) Hu, Q. Y.; Hampsey, J. E.; Jiang, N.; Li, C. J.; Lu, Y. F.; *Chem. Mater.* **2005**, *17*, 1561.

(23) Everett, D. H. *Pure Appl. Chem.* **1972**, *31*, 577.

(24) (a) Thommes, M.; Köhn, R.; Fröba, M. *J. Phys. Chem. B* **2000**, *104*, 7932. (b) Brieler, F. J.; Grundmann, P.; Fröba, M.; Chen, L. M.; Klar, P. J.; Heimbrodt, W.; Krug von Nidda, H.-A.; Kurz, T.; Loidl, A. *J. Am. Chem. Soc.* **2004**, *126*, 797.

(25) Barrett, E. P.; Joyner, L. G.; Halenda, P. P. *J. Am. Chem. Soc.* **1951**, *73*, 373.

(26) Lastokie, C.; Gubbins, K. E.; Quirke, N. *J. Phys. Chem.* **1993**, *97*, 4786.

(27) Thommes, M.; Köhn, R.; Fröba, M. *Appl. Surf. Sci.* **2002**, *196*, 239.

(28) (a) Klink, S. I.; Alink, P. O.; Grave, L.; Peters, F. G. A.; Hofstraat, J. W.; Geurts, F.; van Veggel, F. C. J. M. *J. Chem. Soc., Perkin Trans. 2* **2001**, 363. (b) Lai, W. P. W.; Wong, W. T. *New J. Chem.* **2000**, *24*, 943.

(29) (a) Tsvirko, M. P.; Stelmakh, G. F.; Pyatosin, V. E.; Solovyov, K. N.; Kachura, T. F. *Chem. Phys. Lett.* **1980**, *73*, 80. (b) Quici, S.; Cavazzini, M.; Marzanni, G.; Accorsi, G.; Armaroli, N.; Ventura, B.; Barigelletti, F. *Inorg. Chem.* **2005**, *44*, 529. (c) Sun, L. N.; Zhang, H. J.; Meng, Q. G.; Liu, F. Y.; Fu, L. S.; Peng, C. Y.; Yu, J. B.; Zheng, G. L.; Wang, S. B. *J. Phys. Chem. B* **2005**, *109*, 6174.

(30) Boulon, G.; Collombet, A.; Brenier, A.; Cohen-Adad, M. T.; Yoshikawa, A.; Lebbou, K.; Lee, J. H.; Fukuda, T. *Adv. Funct. Mater.* **2001**, *11*, 263.

(31) (a) Hartmann, M.; Vinu, A. *Langmuir* **2002**, *18*, 8010. (b) Galarneau, A.; Cambon, H.; Renzo, F. D.; Ryoo, R.; Choi, M.; Fajula, F. *New J. Chem.* **2003**, *27*, 73. (c) Ryoo, R.; Ko, C. H.; Kruk, M.; Antochshuk, V.; Jaroniec, M. *J. Phys. Chem. B* **2000**, *104*, 11465. (d) Jun, S.; Joo, S. H.; Ryoo, R.; Kruk, M.; Jaroniec, M.; Liu, Z.; Ohsuna, T.; Terasaki, O. *J. Am. Chem. Soc.* **2000**, *122*, 10712.

(32) Slooff, L. H.; van Blaaderen, A.; Polman, A.; Hebbink, G. A.; Klink, S. I.; Van Veggel, F. C. J. M.; Reinhoudt, D. N.; Hofstraat, J. W. *J. Appl. Phys.* **2002**, *91*, 3955.

(33) Li, H. H.; Inoue, S.; Machida, K. I.; Adachi, G. Y. *Chem. Mater.* **1999**, *11*, 3171.